

Semantic Scene Completion Based 3D Traversability Estimation for Off-Road Terrains

Zitong Chen, Chao Sun, Shida Nie, Chen Min, Changjiu Ning, Haoyu Li, and Bo Wang

Abstract—Off-road environments present significant challenges for autonomous ground vehicles due to the absence of structured roads and the presence of complex obstacles, such as uneven terrain, vegetation, and occlusions. Traditional perception algorithms, designed primarily for structured environments, often fail under these conditions, leading to inaccurate traversability estimations. In this paper, ORDformer, a novel multimodal method that combines LiDAR point clouds with monocular images, is proposed to generate dense traversable occupancy predictions from a forward-facing perspective. By integrating multimodal data, environmental feature extraction is enhanced, which is crucial for accurate occupancy estimation in complex terrains. Furthermore, RELLIS-OCC, a dataset with 3D traversable occupancy annotations, is introduced, incorporating geometric features such as step height, slope, and unevenness. Through a comprehensive analysis of vehicle obstacle-crossing conditions and the incorporation of vehicle body structure constraints, four traversability cost labels are generated: lethal, medium-cost, low-cost, and free. Experimental results demonstrate that ORDformer outperforms existing approaches in 3D traversable area recognition, particularly in off-road environments with irregular geometries and partial occlusions. Specifically, ORDformer achieves over a 20% improvement in scene completion IoU compared to other models. The proposed framework is scalable and adaptable to various vehicle platforms, allowing for adjustments to occupancy grid parameters and the integration of advanced dynamic models for traversability cost estimation.

Note to Practitioners—The motivation of this paper is to help identify areas where vehicles can safely drive in off-road terrains, improving both safety and efficiency in navigation. Current methods typically process semantic and geometric passability features separately, resulting in coarse drivable area recognition. This paper presents ORDformer that combines semantic and geometric features and introduces the RELLIS-OCC dataset specifically for training the model. In real vehicle tests, ORDformer demonstrates effectiveness in challenging off-road scenarios. Future work will integrate ORDformer with 3D path planning algorithms and release datasets with more complex

This work was supported by Key-Area Research and Development Program of Guangdong Province (2023B0909040001), Shenzhen Science and Technology Program (No. KJZD20231023100304010), National Key Research and Development Program (2022YFB2503203). (Corresponding author: Chao Sun.)

Zitong Chen, Chao Sun, Changjiu Ning, Haoyu Li, and Bo Wang are with the Shenzhen Automotive Research Institute, Beijing Institute of Technology, Shenzhen, 518118, China, and also with the School of Mechanical Engineering, Beijing Institute of Technology, Beijing, 100081, China (e-mail: zitongchen2000@163.com; chaosun@bit.edu.cn; ning18500681112@163.com; rabbit.yujixyz@gmail.com; 3120205224@bit.edu.cn).

Shida Nie is with the School of Mechanical Engineering, Beijing Institute of Technology, Beijing, 100081, China, and also with the Advanced Technology Research Institute (Jinan), Beijing Institute of Technology, Jinan, 250307, China (email:nieshida@bit.edu.cn).

Chen Min is with the Research Center for Intelligent Computing Systems, Institute of Computing Technology, Chinese Academy of Sciences, Beijing, 100190, China (e-mail: mincheng@ict.ac.cn).



Fig. 1. Common challenges in off-road scenarios: (a) Irregular geometries formed by rocky piles, and (b) Partial occlusions caused by vegetation.

off-road environments to further improve the adaptability and practicality of autonomous navigation systems. This research is applicable to various types of autonomous ground platforms, offering potential for optimizing vehicle autonomy systems and enhancing traversability performance under complex conditions. This can assist engineers in improving the capability of vehicles to navigate challenging environments.

Index Terms—Traversability estimation, semantic scene completion, multimodal perception fusion, off-road navigation.

I. INTRODUCTION

AUTONOMOUS vehicles are increasingly deployed across various environments, including urban, suburban, and off-road settings. While significant advancements have been made in structured environments with well-defined roads and traffic regulations, navigating unstructured off-road terrains remains a substantial challenge. Off-road environments lack clear pathways and present irregular obstacles, as well as diverse terrain features such as uneven ground, vegetation, and occlusions caused by rocky piles or dense foliage, as shown in Fig. 1. These complexities require advanced perception capabilities to ensure safe and efficient navigation.

In urban environments, datasets such as KITTI [1], nuScenes [2], Waymo Open [3], and ApolloScape [4] provide valuable real-world data for obstacle detection and localization. Traditional perception methods [5]–[8], designed for 3D object detection tasks, detect and localize obstacles, representing them with bounding boxes. However, these methods struggle to identify irregular and continuously distributed objects in off-road conditions. Recent approaches [9]–[12] for 3D occupancy prediction focus on capturing fine-grained spatial structures and semantic information through voxel-based representations. While these methods provide more accurate modeling of obstacles, off-road scenarios also require evaluating the traversability of the environment.

To address these challenges, ORDformer is proposed as a novel multimodal method for off-road traversability esti-

TABLE I
COMPARISON OF DIFFERENT OFF-ROAD ENVIRONMENT DATASET.(PRO.: PROPRIOCEPTIVE, SEG.: SEGMENTATION, DET.: DETECTION, EXC.: EXCITATION, SSD: SELF-SUPERVISED DRIVING, ANN.: ANNOTATION)

Dataset	Year	RGB	Stereo	Depth	NIR	Sensors						Tasks						Size	Ann.	Ann. Type	
						Laser /Lidar	4D Radar	IMU /INS	GPS	Action	Pro.	2D Seg.	3D Seg.	2D Det.	SLAM	Exc.	SSD				
Tong [13]	2013	-	-	-	-	Laser	-	✓	✓	-	-	-	-	-	-	✓	-	-	384	-	-
DeepScene [14]	2016	1024 × 768	-	✓	✓	-	-	-	-	-	-	✓	-	-	-	-	-	15,000	366	pixel-wise	
YCIR [15]	2018	1024 × 544	-	-	-	-	-	-	-	-	-	-	-	-	-	-	-	1,076	1,076	pixel-wise	
RUGD [16]	2019	1376 × 1110	-	-	-	-	-	-	-	-	-	✓	-	-	-	-	-	37,000	7,546	pixel-wise	
Gresenz [17]	2021	3840 × 2160	-	-	-	-	-	-	✓	✓	-	✓	-	-	-	-	✓	12,982	-	-	
RELLIS-3D [18]	2021	1920 × 1200	✓	-	-	32-line/ 64-line	-	✓	-	-	-	✓	✓	-	✓	-	-	6,235 /13,556	6,235 /13,556	pixel-wise /point-wise	
ROOAD [19]	2021	1920 × 1200	-	-	-	-	-	✓	✓	-	-	-	-	-	✓	-	-	20,000	-	-	
CaT [20]	2022	1928 × 1208	-	-	-	-	-	-	-	-	-	✓	-	-	-	-	-	12,300	1,812	traversability	
ORFD [21]	2022	1280 × 720	-	-	-	40-line	-	-	-	-	-	✓	-	-	-	-	-	12,198	12,198	traversability	
SORT [22]	2022	1280 × 720	-	-	-	-	-	-	-	-	-	✓	-	-	-	-	-	20,834	20,834	pixel-wise	
TartanDrive [23]	2022	1024 × 512	✓	✓	-	-	-	✓	✓	✓	✓	-	-	-	✓	-	✓	5 hours	-	-	
WaterScenes [24]	2023	1920 × 1080	-	-	-	-	-	✓	✓	✓	-	✓	✓	✓	-	-	-	54,120 /54,120	54,120 /54,120	pixel-wise/ bounding box /point-wise	
Wild-Places [25]	2023	-	-	-	-	16-line	-	✓	-	-	-	-	-	-	✓	-	-	66,863	-	-	
GOOSE [26]	2024	2448 × 2048	-	-	✓	32-line/ 128-line	-	✓	✓	-	-	✓	✓	-	✓	-	-	15,000 /10,000	10,000 /10,000	pixel-wise /point-wise	
TartanDrive v2.0 [27]	2024	1024 × 512	✓	✓	-	solid/ 32-line	-	✓	✓	✓	✓	-	-	-	✓	✓	✓	7 hours	-	-	

mation. This approach integrates LiDAR point clouds with monocular camera images to generate dense semantic occupancy predictions from a forward-facing perspective. By leveraging the complementary advantages of LiDAR's geometric precision and the rich semantic information provided by camera sensors, ORDformer enhances the extraction of environmental features, which is essential for accurate occupancy estimation in complex terrains.

Furthermore, RELLIS-OCC, a dataset featuring 3D traversable occupancy annotations, is introduced. This dataset encompasses geometric features such as step height, slope, and unevenness, essential for evaluating the relationship between terrain traversability and vehicle dynamics. Through comprehensive analysis of vehicle obstacle-crossing conditions and incorporation of vehicle body structure constraints, a mapping from voxel semantic categories to traversability cost is established, resulting in four traversability cost labels: lethal, medium-cost, low-cost, and free. This mapping provides a detailed understanding of terrain difficulty, offering precise information for autonomous navigation decision-making.

Building upon this foundation, extensive experiments demonstrate that ORDformer significantly outperforms existing approaches in 3D traversable area recognition, especially in off-road environments where obstacles exhibit irregular geometries and are often partially occluded. Specifically, ORDformer achieves over a 20% improvement in the scene completion IoU metric compared to other models. This performance boost underscores the effectiveness of the multimodal fusion and advanced feature extraction techniques.

Moreover, the proposed framework is highly scalable and adaptable to various vehicle platforms. It offers the flexibility to adjust occupancy grid parameters and can incorporate more sophisticated dynamic models for traversability cost estimation. This adaptability ensures that the method can be tailored to the specific geometric and dynamic characteristics of different autonomous vehicles, enhancing their ability to navigate complex off-road environments safely and efficiently.

In summary, the main contributions are as follows:

- ORDformer, a novel framework utilizing a deformable attention mechanism to integrate LiDAR point clouds and monocular images for 3D traversability prediction, is proposed. To our knowledge, this constitutes the first work to employ semantic scene completion for generating environmental traversable occupancy estimations.
- A pipeline for generating 3D traversable occupancy annotations is introduced, alongside the RELLIS-OCC dataset, a 3D semantic occupancy dataset captured from a forward-facing camera perspective. This dataset addresses the existing gap in 3D traversability annotations for off-road environments.
- ORDformer improves the scene completion IoU metric by over 20% compared to existing models, achieving mean IoU scores of 10.50 and 15.70 for semantic and traversability cost annotations, respectively. In real vehicle experiments, ORDformer performs well in complex off-road scenarios.

The rest of the paper is organized as follows. Section II provides a brief review of the relevant literature. Subsequently, the proposed network and dataset is detailed in Section III. Experimental results and discussion are provided in Section IV. Finally, the conclusion is drawn in Section V.

II. RELATED WORKS

A. Off-road Environment Datasets

Perception technology in autonomous driving largely relies on large-scale training datasets; however, existing datasets often do not clearly distinguish between off-road and unstructured road environments. Due to this situation, datasets designed for unstructured roads have been compiled and summarized, as presented in Table I. Public datasets can be categorized based on their data sources into real-vehicle datasets [13]–[21], [23]–[27] and simulation datasets [22]. Due to differences in data acquisition platform configurations, these datasets typically contain image [14]–[16], LiDAR point clouds [13], [25], positioning data [19], or multimodal

data [18], [24]. Notably, the TartanDrive [23] dataset, in addition to multimodal data, includes vehicle behavior data (pedal positions, steering) and vehicle proprioceptive data (suspension travel, wheel speed). Some datasets of unstructured roads include annotation information, which can be divided into semantic annotations [16], [18] and traversable area annotations [20], [21]. The RUGD [16] and RELLIS-3D [18] datasets employ the same labeling rules to annotate the semantic categories of objects in the environment. The CaT [20] and ORFD [21] datasets feature traversable area annotations made by experienced drivers, who subjectively judge based on the type of platform.

B. Traversability Estimation Scheme

Dima et al. [28] defined obstacles as "areas that a vehicle cannot or should not traverse." The initiation of the DARPA Challenge in 2004 significantly advanced research on traversable regions in off-road environments [28]–[33]. Early studies frequently employed Support Vector Machines (SVMs) to recognize vehicle traversable areas using various perception schemes, including LiDAR and vision fusion [34], **pure LiDAR methods** [35], and pure vision approaches [36]. With the development of deep learning, these techniques have been widely applied to off-road research, encompassing traversable area image segmentation [37], [38], road detection and classification [39]–[41], LiDAR point cloud obstacle recognition [42], [43], multi-sensor fusion [44]–[47], and weakly supervised traversable area recognition [48]. Traversable area recognition results are typically represented in various forms, including images [49], 2D grid maps [50], 2.5D grid maps [44], and 3D grid maps [51].

C. Traversability Quantification

Goodin et al. [52] defines "traversability" as a quantification of the drivability of vehicles with certain characteristics on terrain. In off-road scenarios, layered cost maps composed of multiple sub-maps addressing different terrain features are widely used for traversable area analysis [53]. These layers typically include ground semantic and geometric information, making the selection of appropriate cost functions crucial for accurate traversability estimation.

Cameras capture rich semantic scene data, while LiDAR provides precise geometric information; thus, fusing these modalities is a common approach [51], [54]. Zhao et al. [54] integrated images and LiDAR point clouds to construct an elevation-semantic 2D grid map, assigning traversability probabilities to various semantic categories to generate a traversability probability grid. Leung et al. [55] developed a traversability cost map by combining image-based semantic segmentation with geometric attributes such as slope, step height, and roughness. Shaban et al. [43] classified point clouds into four traversability levels: free passage, low cost, medium cost, and obstacles, using deep learning networks to produce a Bird's Eye View (BEV) traversability map.

III. METHODS

The objective is to predict a dense semantic scene within the camera view in front of the platform by leveraging

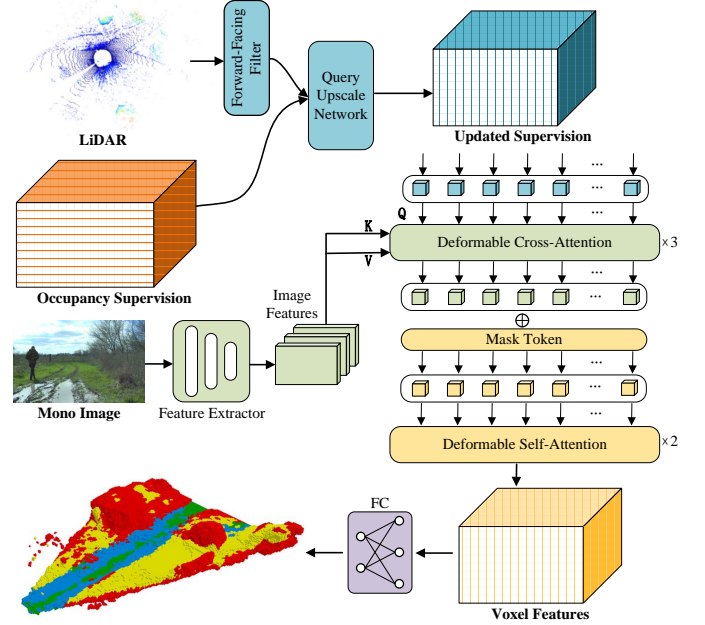


Fig. 2. Overall framework of ORDformer.

monocular images and LiDAR point clouds as input, thereby enabling accurate and reliable traversability estimation in off-road environments. Specifically, the image I_t and LiDAR point cloud L_t are taken as inputs, and the output is a voxel grid $Y_t \in \{c_0, c_1, c_2, \dots, c_M\}^{H \times W \times Z}$, where each voxel is classified as either empty $\{c_0\}$ or occupied by a specific traversability class within $\{c_1, c_2, \dots, c_M\}$. In this context, M denotes the total number of traversability classes, while H , W , and Z represent the length, width, and height of the voxel grid, respectively. To facilitate this process, RELLIS-OCC, the first occupancy dataset with traversability cost annotations specifically designed for off-road scenarios, is introduced.

A. Architecture of ORDformer

Off-road environments lack structured roads and traffic regulation information, making the traversability of such terrains closely linked to the geometric constraints of the platform and necessitating detailed geometric ground analysis. Consequently, there is an increased demand for advanced 3D occupancy prediction capabilities in perception algorithms. To address these challenges, a multimodal semantic scene completion method specifically designed for off-road conditions is proposed. This method leverages LiDAR point clouds and monocular images to generate dense semantic occupancy predictions from a forward-facing perspective. The overall pipeline of ORDformer is illustrated in Fig. 2.

The model begins by extracting features from both modalities: the LiDAR data, which provides precise geometric information, and images, which contribute rich semantic details. These features are then fused using deformable attention mechanisms to effectively integrate spatial and semantic information. Subsequently, the fused features are processed through deformable self-attention layers to enhance the 3D occupancy

representation. Finally, this results in a dense occupancy map highlighting traversable areas.

1) *Feature Extraction*: To achieve more accurate occupancy estimations, multimodal information is utilized to extract environmental features. The model employs a ResNet-50 backbone to extract image features $F_t^{2D} \in \mathbb{R}^{l \times b \times d}$ from the monocular camera image I_t , where $l \times b$ represents the spatial resolution and d denotes the feature dimension. Concurrently, the sparse point clouds L_t from the LiDAR input are voxelized to generate sparse voxel occupancy supervision $S_{\text{spa}} \in \{0, 1\}^{H \times W \times Z}$. Subsequently, a query upscale network is utilized to produce lower spatial resolution occupancy supervision $S_{\text{den}} \in \{0, 1\}^{H/2 \times W/2 \times Z/2}$, thereby enhancing the robustness of the queries.

Mask Token. The mask token module proposed by Y. Li [56] is incorporated to represent empty voxel spaces within the environment. When combined with voxel occupancy supervision, this approach forms a more comprehensive 3D voxel feature, facilitating improved occupancy predictions.

2) *Feature Fusion*: In the model, deformable attention (DA) mechanisms [57] are adopted to facilitate the interaction between local regions of interest in the 3D and 2D feature spaces. Deformable attention dynamically samples N_s points around a reference point, and the attention weights are adaptively learned based on the query vector, while the spatial offsets for sampled points are predicted relative to the reference point, enabling flexible and efficient feature aggregation. The attention results are computed based on these samples using the following equation:

$$\text{DA}(q, p, F) = \sum_{s=1}^{N_s} A_s W_s F(p + \delta p_s), \quad (1)$$

where, q is the query vector, p denotes the reference point associated with q , F represents the input feature map, $W_s \in \mathbb{R}^{d \times d}$ are learnable weight matrices for value generation at each sampled point, $A_s \in [0, 1]$ are attention weights for each sampled point, dynamically learned based on the query, $\delta p_s \in \mathbb{R}^2$ are the predicted offsets for the sampled points relative to the reference point p , and $F(p + \delta p_s)$ denotes the feature vector at the location $p + \delta p_s$, extracted via bilinear interpolation from the input features.

Deformable Cross-Attention (DCA). Multiple DCA layers are employed to enhance the interaction between the occupancy supervision queries S_{den} and the image features F_t^{2D} , thereby facilitating the integration of multimodal information. The 3D grids are projected onto the 2D image feature space F_t^{2D} using projection matrices. The resulting 2D points serve as reference points for the queries S_{den} , from which surrounding features are sampled. A weighted sum of the sampled features is computed to produce the output of the DCA layers. Consequently, refined queries \hat{S}_{den} are obtained, fusing environmental semantic features with geometric features.

$$\text{DCA}(s_{\text{den}}, F_t^{2D}) = \text{DA}(s_{\text{den}}, \mathcal{P}(p, t), F_t^{2D}), \quad (2)$$

for each query s_{den} at position $p = (x, y, z)$, the camera projection function $\mathcal{P}(p, t)$ is applied to map the query to a corresponding reference point on the image I_t .

Deformable Self-Attention (DSA). The refined queries \hat{S}_{den} are concatenated with mask tokens to form the initial voxel features $F^{3D} \in \mathbb{R}^{H/2 \times W/2 \times Z/2 \times d}$. Subsequently, these features are processed through multiple DSA layers to obtain the enhanced voxel features $\hat{F}^{3D} \in \mathbb{R}^{H/2 \times W/2 \times Z/2 \times d}$. The DSA layers enable the model to learn spatial 3D occupancy features more efficiently and accurately. In the equations, the query q_p can be either a mask token or a refined query located at position $p = (x, y, z)$.

$$\text{DSA}(F^{3D}, F^{3D}) = \text{DA}(q_p, p, F^{3D}). \quad (3)$$

3) *Output*: The enhanced voxel features \hat{F}^{3D} are input to fully connected (FC) layers and passed through a softmax function to produce dense semantic occupancy predictions $Y_t \in \{c_0, c_1, c_2, \dots, c_M\}^{H \times W \times Z}$, where each voxel is classified as either empty $\{c_0\}$ or occupied by a specific traversability class within $\{c_1, c_2, \dots, c_M\}$. Mapping these predictions back to the 3D grid yields a detailed occupancy map that highlights traversable areas and provides semantic labels essential for autonomous off-road navigation.

4) *Training Loss*: ORDformer is trained end-to-end from scratch by minimizing three primary loss components: the semantic scale loss $\mathcal{L}_{\text{scal}}^{\text{sem}}$, the geometric scale loss $\mathcal{L}_{\text{scal}}^{\text{geo}}$, and the weighted cross-entropy loss \mathcal{L}_{ce} . The total training loss $\mathcal{L}_{\text{total}}$ is defined as the sum of these individual losses:

$$\mathcal{L}_{\text{total}} = \mathcal{L}_{\text{ce}} + \mathcal{L}_{\text{scal}}^{\text{sem}} + \mathcal{L}_{\text{scal}}^{\text{geo}}. \quad (4)$$

The weighted cross-entropy loss is computed as follows:

$$\mathcal{L}_{\text{ce}} = \frac{1}{\Omega} \sum_{i \in \Omega} \omega_{\text{tar}_i} \left(y_{i, \text{tar}_i} - \log \left(\sum_{c=1}^M e^{y_{i,c}} \right) \right), \quad (5)$$

where Ω represents the set of valid voxels, M is the number of classes, tar_i denotes the true class of voxel i , ω_{tar_i} is the class weight for the true class tar_i of voxel i , y_{i, tar_i} is the logit output of the model for the true class tar_i , and $y_{i,c}$ is the logit output of the model predicting voxel i as class c .

In the context of semantic scene completion, model performance is evaluated using several metrics, including Precision P_c , Recall R_c , and Specificity S_c . These metrics assess the ability of the model to correctly classify occupied and non-occupied voxels. The metrics are formulated as follows:

$$P_c(\text{tar}, p) = \log \left(\frac{\sum_{i \in \Omega} p_{i,c} \cdot [\![\text{tar}_i = c]\!]}{\sum_{i \in \Omega} p_{i,c}} \right), \quad (6)$$

$$R_c(\text{tar}, p) = \log \left(\frac{\sum_{i \in \Omega} p_{i,c} \cdot [\![\text{tar}_i = c]\!]}{\sum_{i \in \Omega} [\![\text{tar}_i = c]\!]} \right), \quad (7)$$

$$S_c(\text{tar}, p) = \log \left(\frac{\sum_{i \in \Omega} (1 - p_{i,c}) \cdot [\![\text{tar}_i \neq c]\!]}{\sum_{i \in \Omega} [\![\text{tar}_i \neq c]\!]} \right), \quad (8)$$

where, $p_{i,c}$ represents the predicted probability that voxel i belongs to class c , and $[\![\cdot]\!]$ denotes the Iverson bracket.

For greater generality, the scale loss $\mathcal{L}_{\text{scal}}$ maximizes the above class-wise metrics:

$$\mathcal{L}_{\text{scal}}(\text{tar}, p) = -\frac{1}{M} \sum_{c=1}^M (P_c(\text{tar}, p) + R_c(\text{tar}, p) + S_c(\text{tar}, p)). \quad (9)$$

Based on the formulation, we compute the semantic loss $\mathcal{L}_{\text{scal}}^{\text{sem}} = \mathcal{L}_{\text{scal}}(\text{tar}_{\text{sem}}, p_{\text{sem}})$ and the geometric loss $\mathcal{L}_{\text{scal}}^{\text{geo}} = \mathcal{L}_{\text{scal}}(\text{tar}_{\text{geo}}, p_{\text{geo}})$, where tar_{sem} and tar_{geo} represent the ground truth labels for semantics and geometry, respectively, with p_{sem} and p_{geo} denoting the corresponding model predictions.

B. 3D Traversable Occupancy Annotations

The RELLIS-OCC dataset with 3D traversable occupancy annotations is generated based on the RELLIS-3D dataset [18], comprising five sequences and a total of 11,201 frames. In this context, sequences numbered 00000 to 00003 are designated as the training set, while sequence 00004 is utilized as the validation set.

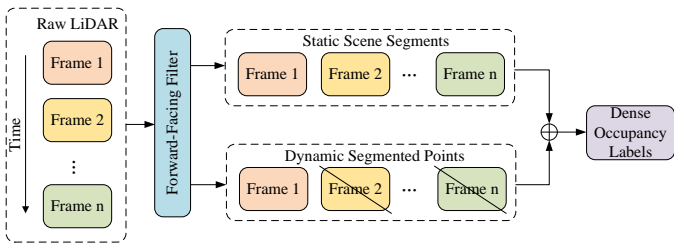


Fig. 3. Dense occupancy ground truth generation.

1) Dense Semantic Occupancy Annotations: In the experiments, networks trained with sparse LiDAR points fail to predict sufficiently dense occupancy, highlighting the need for dense occupancy labels. Dense forward-facing labels are generated from the semantically annotated point clouds of the RELLIS-3D dataset, as shown in Fig. 3. The method transforms multi-frame LiDAR point sequences into a unified coordinate system and voxelizes the dense points into grids, including dynamic objects. This process also captures surface occupancy information since LiDAR scans surface points.

Due to the complex and occluded nature of off-road obstacles, occupancy ground truth within a range of [38.4 m, 51.2 m, 8 m] is selected. The prediction range is set to [0 m, 38.4 m] along the X-axis, [-25.6 m, 25.6 m] along the Y-axis, and [-2 m, 6 m] along the Z-axis. The ground truth is voxelized into a $192 \times 256 \times 40$ grid with a voxel size of 0.2 m and data is filtered to retain voxels within the camera's field of

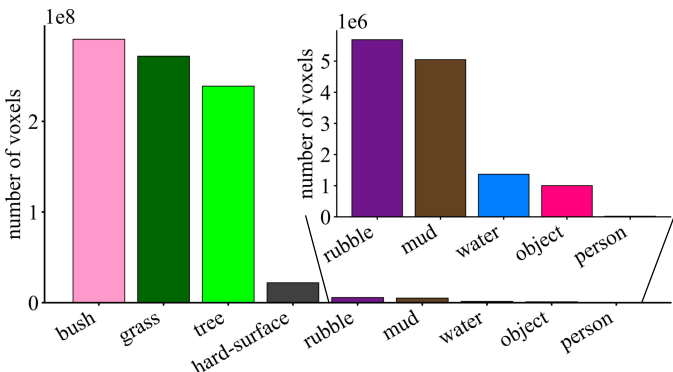


Fig. 4. Voxel Semantic Label Distribution: Grass, trees, and bushes constitute the major classes among the nine valid semantic classes. Each category's color corresponds to its semantic label.

view. A remapping of the original categories is then performed to assess their impact on traversability. Voxel data statistics for the RELLIS-OCC dataset, comprising 10 semantic category labels (including void), are presented in Fig. 4.

2) Geometric Feature Parameter Calculation: A 3D occupancy voxel is constructed by integrating registered dense point clouds. Each voxel $G_j = \{x_j, y_j, z_j\}$ is centered at coordinates (x_j, y_j) in the ground map system and has an elevation z_j . The neighborhood of each voxel is defined as a circular region Ω around G_j , where the point distribution approximates a circle. Each point from the registered dense point cloud is assigned to a voxel, and all points within a voxel form a matrix \mathbf{g} .

$$\mathbf{g} = \begin{bmatrix} x_1 & x_2 & x_3 & \cdots & x_n \\ y_1 & y_2 & y_3 & \cdots & y_n \\ z_1 & z_2 & z_3 & \cdots & z_n \end{bmatrix}. \quad (10)$$

Step Height h : The maximum elevation difference between the central voxel G and other voxels G_j within its neighborhood Ω is calculated to assess the variation in terrain height around the central voxel.

$$h = \max \left(|G^z - G_j^z| \right), \quad G_j \in \Omega, \quad (11)$$

where, G^z and G_j^z represent the elevations of the central voxel G and the neighboring voxel G_j , respectively.

Slope s : The slope is calculated from the elevation values within the neighborhood. For each voxel G , the centers of all voxels in its neighborhood Ω are fitted to a plane. The angle between the normal vector \mathbf{n} of this plane and the unit vector $\mathbf{Z} = (0, 0, 1)$ along the Z-axis of the map coordinate system is defined as the slope.

$$s = \arccos \frac{\mathbf{n} \cdot \mathbf{Z}}{\|\mathbf{n}\| \|\mathbf{Z}\|}, \quad (12)$$

where, the value of n is obtained by calculating the covariance matrix using Principal Component Analysis (PCA).

Unevenness u : The unevenness is estimated by calculating the logarithmic mean squared error (MSE) between the actual elevation of each voxel within the neighborhood Ω and the fitted plane. The unevenness is expressed as:

$$u = \log \left(\frac{1}{m} \sum_{i=1}^m [z_{\text{actual}} - (a_0 \cdot x + a_1 \cdot y + c)]_i^2 \right), \quad m \in \Omega, \quad (13)$$

where, a_0 and a_1 are the coefficients representing the slope in the x and y directions, respectively, and c is the intercept, z_{actual} represents the actual elevation of the current voxel.

3) *Vehicle Obstacle Crossing Condition Analysis:* In off-road conditions, the traversable area of a vehicle is strongly coupled with its geometric passability, as the difficulty of traversing the ground relates to various road geometric features. An analysis of the failure conditions for vehicle obstacle crossing, based on the principles of vehicle ground mechanics, results in the creation of the Step Mask.

Step Mask: The failure conditions for vehicle obstacle crossing include body suspension, front-end collision, vertical obstacles, ditches, and lateral tipping. Since the dataset does

not encompass particularly challenging scenarios, the analysis is focused on four specific cases: overcoming vertical obstacles, crossing ditches, crossing overhang obstacles and traversing longitudinal slopes [58].

a) Vehicle Vertical Obstacle Overcoming Conditions:

The performance of wheeled vehicles in overcoming step-like obstacles and vertical protrusions is primarily evaluated based on the maximum height of vertical obstacles they can surmount. The dimensionless expression for the maximum obstacle height that the front wheels of a 4x4 wheeled vehicle can overcome is:

$$\frac{h}{r} = \frac{1 - \mu \frac{r}{l} + \eta^2 - \eta \sqrt{1 - 2\mu \frac{r}{l} + \eta^2}}{(1 + \mu \frac{r}{l})^2 + \eta^2}. \quad (14)$$

$$\eta = \frac{1 - \mu \frac{r}{l} - (1 + \mu^2) \frac{a}{l}}{\mu}. \quad (15)$$

where, h represents the height of the step obstacle, r represents the wheel radius, μ represents the coefficient of friction, l represents the wheelbase of the vehicle, a represents the horizontal distance from the front axle to the center of gravity of the vehicle.

b) Vehicle Traversing Trenches Conditions: The width of the trenches that a wheeled vehicle can overcome is evaluated using the ratio of the trench width l_d to the wheel diameter D , expressed as $\frac{l_d}{D}$. The ratio of the height of vertical obstacles that can be overcome to the wheel diameter, expressed as $\frac{h}{D}$, can be converted to $\frac{l_d}{D}$, as shown in Equation 16. Given a specific obstacle height h , the corresponding trench width ratio $\frac{l_d}{D}$ can be determined.

$$\frac{l_d}{D} = 2\sqrt{\frac{h}{D} - \left(\frac{h}{D}\right)^2}. \quad (16)$$

c) Vehicle Crossing Overhang Obstacles Conditions:

For a vehicle to successfully traverse overhang obstacles, the height h_{obj} of the lowest point of the obstacle above the ground must exceed the sum of h_{pc} , which is the height of the obstacle point cloud relative to the LiDAR sensor, and h_{Lid} , the height of the LiDAR sensor above the ground. When the vehicle encounters an overhang obstacle, the following conditions must be met:

$$h_{obj} > h_{pc} + h_{Lid}. \quad (17)$$

d) Vehicle Traversing Longitudinal Slopes Conditions:

For traversing longitudinal slopes, the ground platform must satisfy the following condition:

$$\theta_{max} > \alpha, \quad (18)$$

where θ_{max} represents the maximum climbing angle that the vehicle can handle, and α represents the current slope angle of the terrain.

4) Traversability Cost Occupancy Annotations: Rules are established to create an initial mapping from voxel semantic categories to traversability cost, with adjustments made based on the previously computed Step Mask. The Step Mask is determined by evaluating the geometric passability of the vehicle. Voxels not meeting the geometric passability criteria

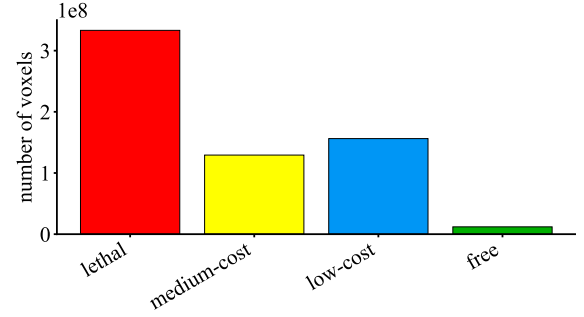


Fig. 5. Voxel traversability cost label distribution: Each category's color corresponds to its traversability cost label.

are assigned a lethal cost. Finally, four traversability cost labels are derived: lethal, medium-cost, low-cost, and free, ranging from difficult to easy traversability. Fig. 5 illustrates the statistical distribution of the traversability cost labels.

C. Architecture of ORD-BKI

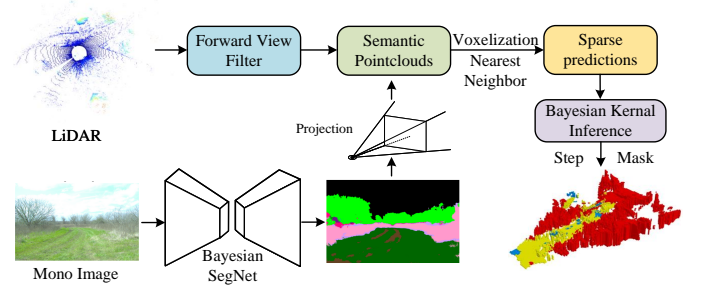


Fig. 6. Overall framework of ORD-BKI.

The research presented in [59] introduces the S-BKI model, which infers grid attributes for discrete semantic grid maps to achieve continuous and dense semantic mapping. To enable a fair comparison, the S-BKI model is built upon, utilizing LiDAR point clouds as input. Based on the vehicle's geometric passability, a feasible domain recognition model, ORD-BKI, is developed, which employs Bayesian Kernel Inference for semantic scene completion, as illustrated in Fig. 6.

The ORD-BKI model utilizes the Bayesian SegNet [60] network to extract semantic information from images, capturing the uncertainty of pixel-wise semantic segmentation. As shown in Fig. 7, the boundaries of road edges and vegetation with varying traversability in off-road environments are often ambiguous, prompting the choice of a network with uncertainty extraction capabilities to enhance the robustness of environmental recognition.

The image semantic segmentation results are projected onto the point clouds to obtain semantically enriched point clouds. Due to the discrete and sparse nature of LiDAR point clouds, it is essential to model the distribution of grid semantic attributes during voxelization to infer the semantic attributes of neighboring grids [59]. The ORD-BKI model employs Bayesian Kernel Inference for semantic scene completion, approximating a Gaussian process, which reduces the time complexity from cubic to linear complexity [61]. The Nearest

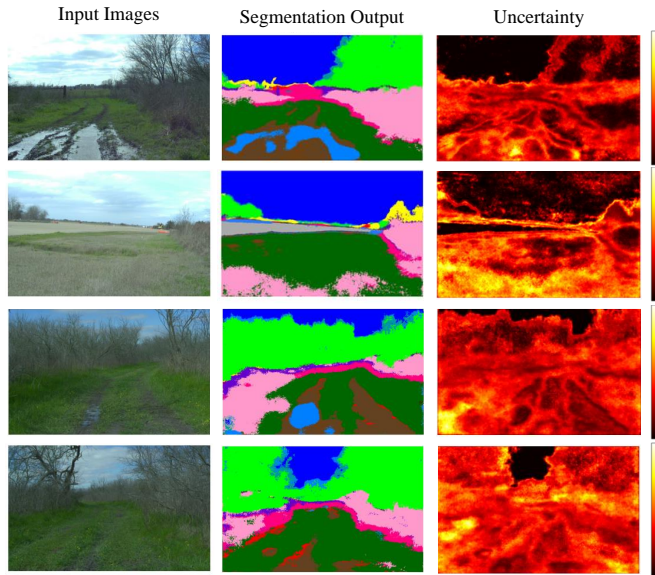


Fig. 7. Uncertainty estimation results on the RELLIS-3D Dataset.

Neighbor algorithm is then used to assign semantics, generating dense semantic occupancy results. The model utilizes an anisotropic kernel function for inference and analyzes the model results under historical frame point cloud inputs. The geometric passability analysis method employed by the model is consistent with the discussions presented earlier in the article.

The anisotropic kernel function is as follows:

$$K(x, \hat{x}) = e^{-\frac{1}{2}d_M^2}, \quad (19)$$

where d_M represents the Mahalanobis distance, calculated using the formula:

$$d_M = \sqrt{(x - \hat{x})^T S^{-1} (x - \hat{x})}. \quad (20)$$

IV. EXPERIMENTS

A. Quantitative Analysis

Experiments are conducted on the RELLIS-OCC dataset for the tasks of 3D semantic occupancy prediction and 3D traversability cost estimation, with the results compared to those obtained by the algorithms presented in [59], [62]–[64]. Due to GPU memory constraints, the Monoscene model is trained on $4 \times V100$ GPUs, while the other models are trained on 4×3090 GPUs. A consistent batch size of 4 is maintained, and each model is trained for 20 epochs.

Evaluation Metrics: The RELLIS-OCC dataset comprises both semantic labels and traversability cost annotations. The traversability cost estimation task is framed as a semantic occupancy prediction task, encompassing four categories: lethal, medium-cost, low-cost, and free. Consequently, traditional metrics employed in 3D semantic occupancy prediction tasks are utilized for evaluation. For the scene completion (SC) task, the Intersection over Union (IoU) of occupied voxels, disregarding their semantic classes, is used as the evaluation metric. For the semantic scene completion (SSC) task, the IoU

of each semantic class and the mean IoU (mIoU) across all semantic classes are adopted as evaluation metrics.

The IoU is defined as:

$$\text{IoU} = \frac{\text{TP}}{\text{TP} + \text{FP} + \text{FN}}. \quad (21)$$

The mIoU across C classes is calculated as:

$$\text{mIoU} = \frac{1}{C} \sum_{i=1}^C \frac{\text{TP}_i}{\text{TP}_i + \text{FP}_i + \text{FN}_i}, \quad (22)$$

where TP, FP, and FN represent the number of true positive, false positive, and false negative predictions, respectively, and C is the number of classes.

1) 3D Semantic Occupancy Prediction: The results of the 3D semantic occupancy prediction task are presented in Table II. To ensure a fair comparison, all methods are evaluated using consistent perception ranges and voxel sizes. Fig. 4 illustrates the distribution statistics for voxel labels within the dataset. The limited availability of ground truth training data for categories such as person and object poses significant challenges for many models in accurately recognizing these classes. Additionally, the RELLIS-3D dataset, which serves as the foundation for RELLIS-OCC dataset, was collected in a campus environment with very limited overlap between sequences. This, combined with the rarity of hard-surface scenes in the validation set, leads to generally lower recognition metrics for the hard-surface category.

Despite these challenges, ORDformer demonstrates superior performance across a wide range of categories. Notably, it achieves state-of-the-art results in identifying tree and bush, with IoU scores of 37.09 and 23.65, respectively. Furthermore, while many models struggle with challenging classes such as mud, ORDformer achieves an IoU of 10.34, significantly higher than competing approaches. Most impressively, ORDformer outperforms other models by over 20% in the scene completion (SC) IoU metric, achieving a score of 50.20 compared to the second-best result of 38.64 from SSCNet-full. These results underscore the effectiveness of ORDformer in integrating multimodal data and performing robust occupancy predictions in complex environments.

2) 3D Traversability Cost Estimation: The results of the 3D Traversability Cost Estimation task are presented in Table III. Across all methods, those based on semantic scene completion outperform the ORD-BKI method, which relies on Bayesian Kernel Inference. This underscores the effectiveness of semantic scene completion approaches in enhancing off-road traversable area recognition. Notably, methods using only LiDAR point clouds as input, such as LMSCNet and SSCNet, exhibit inferior performance in the traversability cost estimation task compared to models that incorporate camera input. This suggests that image input is indispensable for accurate traversability cost estimation.

Our investigation reveals that while methods employing image-to-point cloud semantic mapping are widely used for traversable area recognition tasks [45], [51], [59], there is a lack of quantitative evaluation of their environmental perception results. Taking the ORD-BKI method as an example, a quantitative analysis of its perception performance

TABLE II
MONOCULAR SEMANTIC SCENE COMPLETION RESULTS ON THE RELLIS-OCC DATASET.

Method	Grass	Tree	Hard-surface	Object	SSC					SSC mIoU	SC IoU
					Bush	Water	Person	Mud	Rubble		
Monoscene [62]	27.99	11.12	0.000	1.04	18.11	3.28	0.001	3.33	16.50	8.14	33.15
SSCNet [63]	22.74	33.92	0.000	6.59	17.22	13.71	0.000	0.000	26.41	12.06	33.99
SSCNet-full [63]	30.19	33.49	0.000	4.22	19.29	19.30	0.001	0.001	29.5	13.61	38.64
LMSNet [64]	16.34	33.12	0.000	0.000	19.33	0.000	0.000	0.000	14.31	8.31	31.48
LMSNet-SS [64]	8.94	36.13	0.000	0.000	18.74	0.000	0.000	0.000	0.000	6.38	33.22
ORDformer(Ours)	25.47	37.09	0.008	2.05	23.65	3.81	0.006	10.34	2.59	10.50	50.20

TABLE III
MONOCULAR TRAVERSABILITY ESTIMATE RESULTS ON THE RELLIS-OCC DATASET.(M-COST: MEDIUM-COST, L-COST: LOW-COST)

Method	Lethal	SSC			SSC mIoU	SC IoU
		M-cost	L-cost	Free		
Monoscene [62]	12.07	13.37	27.30	5.51	14.59	34.92
SSCNet [63]	11.58	8.29	13.95	0.004	8.56	23.34
SSCNet-full [63]	11.35	8.34	15.60	0.002	8.86	24.70
LMSNet [64]	2.87	7.32	7.62	0.000	4.45	9.59
LMSNet-SS [64]	1.04	5.87	10.64	0.000	4.39	10.09
ORD-BKI [59]	6.29	0.76	0.85	0.000	1.98	17.47
ORDformer(Ours)	19.98	13.89	23.50	5.41	15.70	49.78

is conducted by setting the parameter k in the Bayesian Kernel Inference to 8. To assess the effect of the Bayesian Kernel Inference module, point clouds are voxelized using only semantic mapping, and evaluations are performed. The comparative results, presented in Table IV, demonstrate that Bayesian Kernel Inference significantly enhances voxel occupancy prediction. Nevertheless, since the inference relies solely on voxelized grids of sparse point clouds, all metrics of the ORD-BKI model remain substantially lower than those of the semantic scene completion-based approach.

TABLE IV
IMPACT OF BAYESIAN KERNEL INFERENCE ON SEMANTIC MAPPING.

Method	SSC mIoU	SC IoU
ORD-BKI	2.03	14.48
Semantic-Projection	0.25	1.5

Notably, ORDformer achieves state-of-the-art results in the lethal and medium-cost categories, with IoU scores of 19.98 and 13.89, respectively. Specifically, in the lethal traversability category, ORDformer attains an IoU score of 19.98, which is 7.91 IoU higher than that of the second-best model, Monoscene. Furthermore, in the free and low-cost categories, ORDformer delivers competitive performance. The overall SSC mIoU and SC IoU scores are 15.70 and 49.78, respectively. These results represent significant improvements of over 20% in SC IoU compared to other methods, underscoring the excellent performance of ORDformer in occupancy prediction. Importantly, the enhanced geometric perception capabilities of ORDformer are critical for identifying complex negative and overhanging obstacles in off-road environments, where accurate 3D traversability estimation is crucial for safe navigation.

B. Qualitative Analysis

Visualization of traversability prediction results from different models is presented in Fig. 8. By comparing these results with the ground truth, it is evident that ORDformer effectively identifies road traversability challenges in off-road environments. Additionally, the model accurately infers and completes regions containing vegetation and other obstacles.

As illustrated in Fig. 9, a pile of rocks appears in front of the platform. Remarkably, the model effectively recognizes the rocky pile as impassable and accurately assesses its spatial distribution. Although the ground truth data designates the edges of the rocky obstacles as lethal regions, it incorrectly assigns labels to the flat areas within the rocky pile. Nevertheless, the model correctly infers the entire rocky pile as lethal, demonstrating its generalization capabilities.

In off-road scenarios, trees are among the most common obstacles that ground unmanned platforms must avoid during trajectory planning. Therefore, accurate detection of trees is essential. Fig. 10 illustrates the detection results of ORDformer for multiple consecutively distributed trees. Different colored bounding boxes indicate the correspondence between various trees in images captured at different times, the ground truth, and traversability estimation results. By accurately identifying the spatial distribution of trees within the effective detection range, ORDformer ensures that ground unmanned platforms can effectively avoid these common obstacles in off-road environments, thereby facilitating safe trajectory planning.

The inference results of the ORD-BKI model are visualized, as shown in Fig. 11. The results demonstrate that although the ORD-BKI model effectively identifies traversable ground areas in the two-dimensional plane, its performance in representing the 3D environment is suboptimal. This observation suggests that semantic mapping approaches are significantly influenced by the density of LiDAR point clouds. Such approaches are more suitable for platforms equipped with multiple supplementary blind-spot LiDARs. In contrast, unmanned platforms equipped with only a single LiDAR sensor experience limitations in representational performance for 3D traversable area recognition tasks due to the low point cloud density within the field of view of the camera.

Ground surfaces become partially exposed due to vehicle passage, resulting in the formation of ruts. These rutted areas typically exhibit sparse weed distribution and lack clear boundaries with the surrounding densely weed-covered regions. Their characteristics lie between dirt and grass, which poses

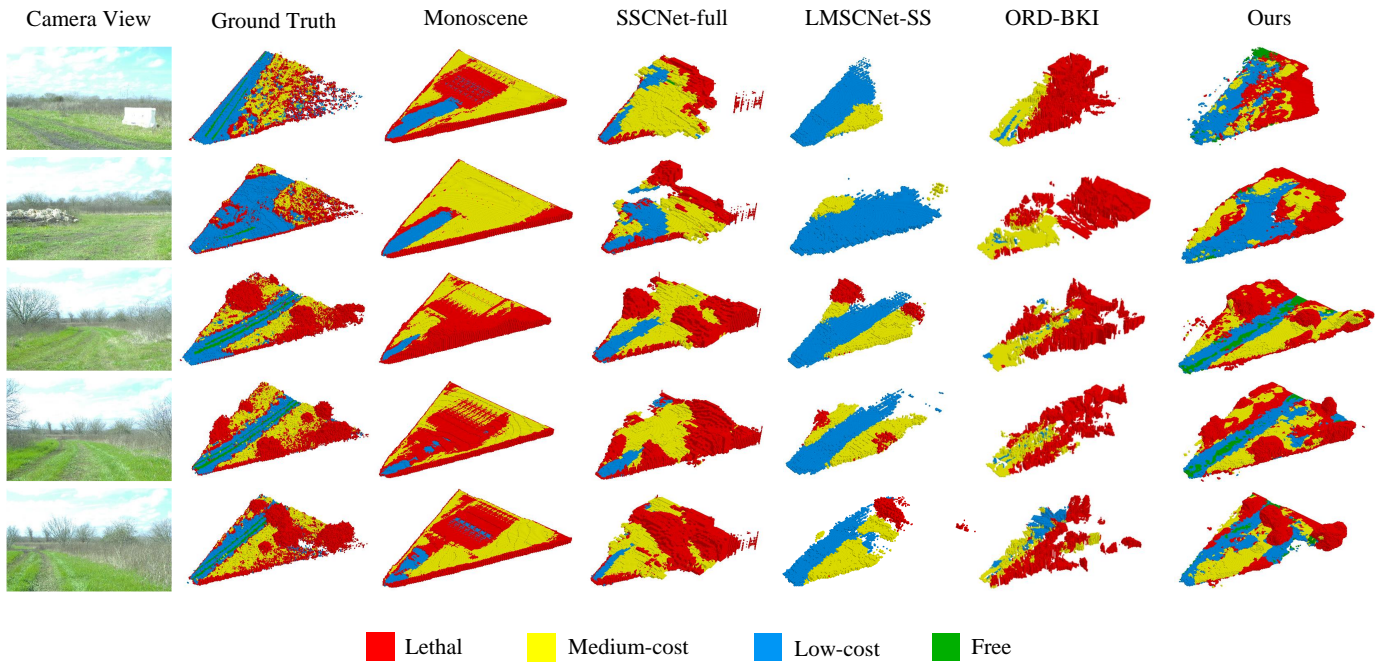


Fig. 8. Visualization of traversability prediction results from different models. From left to right: camera views, ground truth, predictions from the main algorithm (columns 3-6), and traversability estimations from ORDformer.”

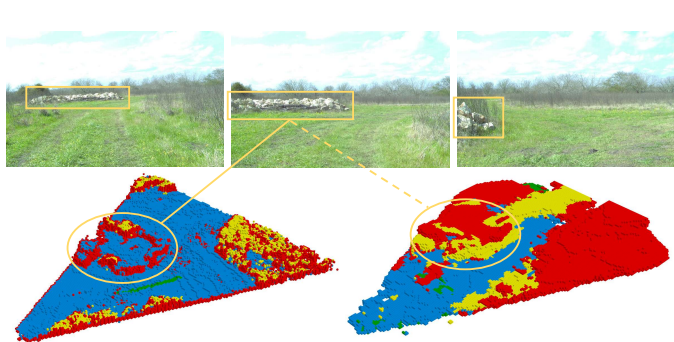


Fig. 9. Detection of rocky piles. Top images: camera views 10 seconds before (left), at the current time (center), and 10 seconds after (right). Bottom images: ground truth (left) and traversability estimations from ORDformer (right).

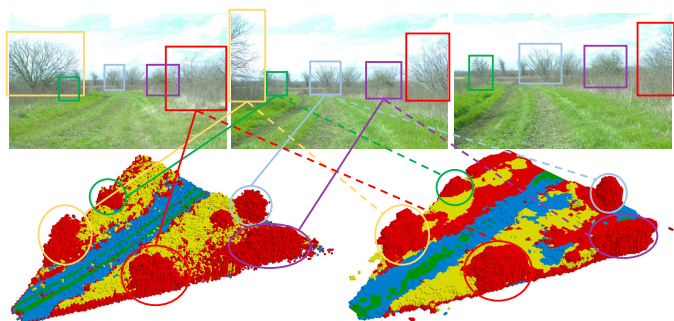


Fig. 10. Detection of multiple consecutive trees. Top images: camera views 10 seconds before (left), at the current time (center), and 10 seconds after (right). Bottom images: ground truth (left) and traversability estimations from ORDformer (right).

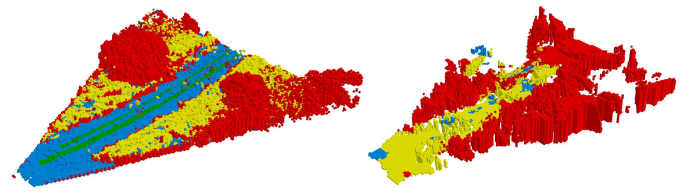


Fig. 11. Ground truth (left) and ORD-BKI inference result.

significant challenges for accurate identification. Therefore, the recognition accuracy of ORDformer in these transitional areas requires further improvement.

C. Real Vehicle Experiments

ORDformer is implemented on a real vehicle platform and validated through tests conducted at the Xiaotianshan Professional Outdoor Off-Road Site in Zhangjiakou City, Hebei Province, China. The test vehicle used is a Jeep Grand Cherokee, equipped with a Suteng Innovation 80-line LiDAR and a Senyun Intelligent monocular camera (see Fig. 12).



Fig. 12. Real vehicle test platform.

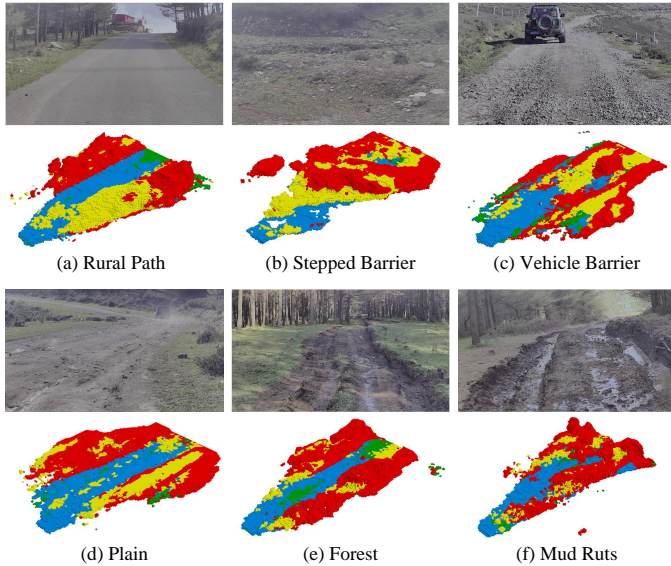


Fig. 13. Real-vehicle test scenarios and model traversability estimation results: (a) Rural Path, (b) Stepped Barrier, (c) Vehicle Barrier, (d) Plain, (e) Forest, and (f) Mud Ruts.



Fig. 14. Effects of intense sunlight on input images: (a) Purple Halos, and (b) Localized Overexposure.

The experiments encompass six typical scenarios: (a) rural roads without ground markings; (b) stepped obstacles composed of scattered rocks and earth mounds; (c) vehicle obstacles present in the direction of travel; (d) wide dirt roads with scattered weeds and shrubs; (e) dirt roads flanked by trees on both sides; and (f) muddy roads filled with deep vehicle ruts. These scenarios simulate diverse challenges in real off-road environments, aiming to evaluate the perception performance and robustness of the algorithm under varying complexities and dynamic conditions.

It is noteworthy that the training data is based on the RELLIS-3D dataset, which is collected using the unmanned ground platform Warthog. However, significant differences exist between the Warthog and the real-vehicle test platform concerning sensor models, vehicle dimensions, and sensor configurations. For instance, the Warthog platform and the Jeep Grand Cherokee differ in vehicle size, as well as in sensor installation heights and angles. These disparities pose challenges to the generalization capability of the algorithm.

Despite these differences, the real-vehicle test results (see Fig. 13) demonstrate that the proposed algorithm accurately identifies the 3D traversability of terrains in off-road environments. This outcome indicates the robust adaptability and generalization capabilities of the algorithm, enabling effective

operation across various sensor configurations and vehicle platforms. During the experiments, it is observed that under intense sunlight conditions (see Fig. 14), the input images exhibit purple halos and localized highlight overexposure effects, leading to incorrect recognitions by the model. Therefore, future work will involve enhancing the robustness of the model to drastic changes in environmental illumination to improve recognition accuracy under challenging lighting scenarios.

V. CONCLUSION

In this paper, We propose ORDformer, a multimodal method for off-road traversability estimation that utilizes LiDAR point clouds and monocular images to generate dense semantic occupancy predictions. By integrating geometric and semantic information, ORDformer enhances environmental feature extraction, enabling more accurate estimation of traversable regions in complex, occluded terrains. Furthermore, we introduce the RELLIS-OCC dataset with 3D traversable occupancy annotations, enabling detailed terrain assessment in off-road environments. Extensive experiments validate the superior performance of ORDformer compared to existing approaches, particularly in handling obstacles with diverse geometries and partial occlusion. ORDformer holds significant potential for real-world deployment, as it can be easily adapted to different vehicle platforms and a range of off-road environments, providing a robust solution for autonomous navigation in challenging conditions.

For future work, the proposed traversability estimation method will be integrated with 3D planning algorithms to enable comprehensive 3D trajectory planning in off-road conditions. Additionally, recognizing the limitations of existing public datasets, we plan to collect an expanded off-road dataset containing complex obstacle information and evaluate the performance of ORDformer in detecting negative and overhanging obstacles.

REFERENCES

- [1] A. Geiger, P. Lenz, C. Stiller, and R. Urtasun, “Vision meets robotics: The kitti dataset,” *The International Journal of Robotics Research*, vol. 32, no. 11, pp. 1231–1237, 2013.
- [2] H. Caesar, V. Bankiti, A. H. Lang, S. Vora, V. E. Lioung, Q. Xu, A. Krishnan, Y. Pan, G. Baldan, and O. Beijbom, “nuscenes: A multimodal dataset for autonomous driving,” in *Proceedings of the IEEE/CVF conference on computer vision and pattern recognition*, pp. 11621–11631, 2020.
- [3] P. Sun, H. Kretzschmar, X. Dotiwalla, A. Chouard, V. Patnaik, P. Tsui, J. Guo, Y. Zhou, Y. Chai, B. Caine, *et al.*, “Scalability in perception for autonomous driving: Waymo open dataset,” in *Proceedings of the IEEE/CVF conference on computer vision and pattern recognition*, pp. 2446–2454, 2020.
- [4] X. Huang, X. Cheng, Q. Geng, B. Cao, D. Zhou, P. Wang, Y. Lin, and R. Yang, “The apolloscope dataset for autonomous driving,” in *Proceedings of the IEEE conference on computer vision and pattern recognition workshops*, pp. 954–960, 2018.
- [5] C. R. Qi, H. Su, K. Mo, and L. J. Guibas, “Pointnet: Deep learning on point sets for 3d classification and segmentation,” in *Proceedings of the IEEE conference on computer vision and pattern recognition*, pp. 652–660, 2017.
- [6] C. R. Qi, L. Yi, H. Su, and L. J. Guibas, “Pointnet++: Deep hierarchical feature learning on point sets in a metric space,” *Advances in neural information processing systems*, vol. 30, 2017.
- [7] S. Shi, Z. Wang, X. Wang, and H. Li, “Part-a² net: 3d part-aware and aggregation neural network for object detection from point cloud,” *arXiv preprint arXiv:1907.03670*, vol. 2, no. 3, 2019.

- [8] Y. Zhou and O. Tuzel, "Voxelnets: End-to-end learning for point cloud based 3d object detection," in *Proceedings of the IEEE conference on computer vision and pattern recognition*, pp. 4490–4499, 2018.
- [9] Y. Huang, W. Zheng, Y. Zhang, J. Zhou, and J. Lu, "Tri-perspective view for vision-based 3d semantic occupancy prediction," in *Proceedings of the IEEE/CVF conference on computer vision and pattern recognition*, pp. 9223–9232, 2023.
- [10] X. Wang, Z. Zhu, W. Xu, Y. Zhang, Y. Wei, X. Chi, Y. Ye, D. Du, J. Lu, and X. Wang, "Openoccupancy: A large scale benchmark for surrounding semantic occupancy perception," in *Proceedings of the IEEE/CVF International Conference on Computer Vision*, pp. 17850–17859, 2023.
- [11] Z. Li, Z. Yu, D. Austin, M. Fang, S. Lan, J. Kautz, and J. M. Alvarez, "Fb-occ: 3d occupancy prediction based on forward-backward view transformation," *arXiv preprint arXiv:2307.01492*, 2023.
- [12] Y. Wei, L. Zhao, W. Zheng, Z. Zhu, J. Zhou, and J. Lu, "Surroundoc: Multi-camera 3d occupancy prediction for autonomous driving," in *Proceedings of the IEEE/CVF International Conference on Computer Vision*, pp. 21729–21740, 2023.
- [13] C. H. Tong, D. Gingras, K. Larose, T. D. Barfoot, and É. Dupuis, "The canadian planetary emulation terrain 3d mapping dataset," *The International Journal of Robotics Research*, vol. 32, no. 4, pp. 389–395, 2013.
- [14] A. Valada, G. L. Oliveira, T. Brox, and W. Burgard, "Deep multi-spectral semantic scene understanding of forested environments using multimodal fusion," in *2016 International Symposium on Experimental Robotics*, pp. 465–477, Springer, 2017.
- [15] D. Maturana, P.-W. Chou, M. Uenoyama, and S. Scherer, "Real-time semantic mapping for autonomous off-road navigation," in *Field and Service Robotics: Results of the 11th International Conference*, pp. 335–350, Springer, 2018.
- [16] M. Wigness, S. Eum, J. G. Rogers, D. Han, and H. Kwon, "A rugged dataset for autonomous navigation and visual perception in unstructured outdoor environments," in *2019 IEEE/RSJ International Conference on Intelligent Robots and Systems (IROS)*, pp. 5000–5007, IEEE, 2019.
- [17] G. Gresenz, J. White, and D. C. Schmidt, "An off-road terrain dataset including images labeled with measures of terrain roughness," in *2021 IEEE International Conference on Autonomous Systems (ICAS)*, pp. 1–5, IEEE, 2021.
- [18] P. Jiang, P. Osteen, M. Wigness, and S. Saripalli, "Rellis-3d dataset: Data, benchmarks and analysis," in *2021 IEEE international conference on robotics and automation (ICRA)*, pp. 1110–1116, IEEE, 2021.
- [19] G. Chustz and S. Saripalli, "Rooad: Rellis off-road odometry analysis dataset," in *2022 IEEE Intelligent Vehicles Symposium (IV)*, pp. 1504–1510, IEEE, 2022.
- [20] S. Sharma, L. Dabbiru, T. Hannis, G. Mason, D. W. Carruth, M. Doude, C. Goodin, C. Hudson, S. Ozier, J. E. Ball, et al., "Cat: Cavs traversability dataset for off-road autonomous driving," *IEEE Access*, vol. 10, pp. 24759–24768, 2022.
- [21] C. Min, W. Jiang, D. Zhao, J. Xu, L. Xiao, Y. Nie, and B. Dai, "Orfd: A dataset and benchmark for off-road freespace detection," in *2022 international conference on robotics and automation (ICRA)*, pp. 2532–2538, IEEE, 2022.
- [22] T. Yan, X. Zheng, W. Liu, B. Liang, and Z. Chen, "The synthetic off-road trail dataset for unmanned motorcycle," in *2022 IEEE 95th Vehicular Technology Conference:(VTC2022-Spring)*, pp. 1–7, IEEE, 2022.
- [23] S. Triest, M. Sivaprakasam, S. J. Wang, W. Wang, A. M. Johnson, and S. Scherer, "Tartandrive: A large-scale dataset for learning off-road dynamics models," in *2022 International Conference on Robotics and Automation (ICRA)*, pp. 2546–2552, IEEE, 2022.
- [24] S. Yao, R. Guan, Z. Wu, Y. Ni, Z. Huang, R. W. Liu, Y. Yue, W. Ding, E. G. Lim, H. Seo, et al., "Waterscenes: A multi-task 4d radar-camera fusion dataset and benchmarks for autonomous driving on water surfaces," *IEEE Transactions on Intelligent Transportation Systems*, 2024.
- [25] J. Knights, K. Vidanapathirana, M. Ramezani, S. Sridharan, C. Fookes, and P. Moghadam, "Wild-places: A large-scale dataset for lidar place recognition in unstructured natural environments," in *2023 IEEE international conference on robotics and automation (ICRA)*, pp. 11322–11328, IEEE, 2023.
- [26] P. Mortimer, R. Hagmanns, M. Granero, T. Luettel, J. Petereit, and H.-J. Wuensche, "The goose dataset for perception in unstructured environments," in *2024 IEEE International Conference on Robotics and Automation (ICRA)*, pp. 14838–14844, IEEE, 2024.
- [27] M. Sivaprakasam, P. Maheshwari, M. G. Castro, S. Triest, M. Nye, S. Willits, A. Saba, W. Wang, and S. Scherer, "Tartandrive 2.0: More modalities and better infrastructure to further self-supervised learning research in off-road driving tasks," *arXiv preprint arXiv:2402.01913*, 2024.
- [28] C. S. Dima, N. Vandapel, and M. Hebert, "Classifier fusion for outdoor obstacle detection," in *IEEE International Conference on Robotics and Automation, 2004. Proceedings. ICRA'04. 2004*, vol. 1, pp. 665–671, IEEE, 2004.
- [29] D. Bradley, S. Thayer, A. Stentz, and P. Rander, "Vegetation detection for mobile robot navigation," *Robotics Institute, Carnegie Mellon University, Pittsburgh, PA, Tech. Rep. CMU-RI-TR-04-12*, 2004.
- [30] A. Huertas, L. Matthies, and A. Rankin, "Stereo-based tree traversability analysis for autonomous off-road navigation," in *2005 Seventh IEEE Workshops on Applications of Computer Vision (WACV/MOTION'05)-Volume 1*, vol. 1, pp. 210–217, IEEE, 2005.
- [31] A. Broggi, C. Caraffi, R. I. Fedriga, and P. Grisleri, "Obstacle detection with stereo vision for off-road vehicle navigation," in *2005 IEEE Computer Society Conference on Computer Vision and Pattern Recognition (CVPR'05)-Workshops*, pp. 65–65, IEEE, 2005.
- [32] R. Manduchi, A. Castano, A. Talukder, and L. Matthies, "Obstacle detection and terrain classification for autonomous off-road navigation," *Autonomous robots*, vol. 18, pp. 81–102, 2005.
- [33] H. Dahlkamp, A. Kaehler, D. Stavens, S. Thrun, and G. R. Bradski, "Self-supervised monocular road detection in desert terrain," in *Robotics: science and systems*, vol. 38, Philadelphia, 2006.
- [34] J. Sock, J. Kim, J. Min, and K. Kwak, "Probabilistic traversability map generation using 3d-lidar and camera," in *2016 IEEE international conference on robotics and automation (ICRA)*, pp. 5631–5637, IEEE, 2016.
- [35] J. Larson and M. Trivedi, "Lidar based off-road negative obstacle detection and analysis," in *2011 14th International IEEE Conference on Intelligent Transportation Systems (ITSC)*, pp. 192–197, IEEE, 2011.
- [36] Z. W.-J. YANG Jian-Hua and W. Zhao-Hui, "Cooperative multi-robot observation of multiple moving targets based on contribution model," *Pattern Recognition and Artificial Intelligence*, vol. 28, no. 04, pp. 335–343, 2015.
- [37] C. J. Holder and T. P. Breckon, "Learning to drive: End-to-end off-road path prediction," *IEEE Intelligent Transportation Systems Magazine*, vol. 13, no. 2, pp. 217–221, 2019.
- [38] L. Dabbiru, S. Sharma, C. Goodin, S. Ozier, C. Hudson, D. Carruth, M. Doude, G. Mason, and J. Ball, "Traversability mapping in off-road environment using semantic segmentation," in *Autonomous Systems: Sensors, Processing, and Security for Vehicles and Infrastructure 2021*, vol. 11748, pp. 78–83, SPIE, 2021.
- [39] Z. Wang, Z. Xiang, and E. Liu, "Object guided beam steering algorithm for optical phased array (opa) lidar," in *Intelligence Science and Big Data Engineering. Visual Data Engineering: 9th International Conference, IScIDE 2019, Nanjing, China, October 17–20, 2019, Proceedings, Part I* 9, pp. 262–272, Springer, 2019.
- [40] A. Li, Y. Ma, and Y. Peng, "Inertia enhanced visual slam method for position and pose recognition," in *CSAA/IET International Conference on Aircraft Utility Systems (AUS 2020)*, vol. 2020, pp. 341–346, IET, 2020.
- [41] Z.-l. DING, Y.-h. HU, J.-w. GONG, G.-m. XIONG, and C. LÜ, "Adaptive road extraction method in different scene based on deep learning," *Transactions of Beijing Institute of Technology*, vol. 39, no. 11, pp. 1133–1137, 2019.
- [42] L. Dabbiru, C. Goodin, N. Scherrer, and D. Carruth, "Lidar data segmentation in off-road environment using convolutional neural networks (cnn)," *SAE International Journal of Advances and Current Practices in Mobility*, vol. 2, no. 2020-01-0696, pp. 3288–3292, 2020.
- [43] A. Shaban, X. Meng, J. Lee, B. Boots, and D. Fox, "Semantic terrain classification for off-road autonomous driving," in *Conference on Robot Learning*, pp. 619–629, PMLR, 2022.
- [44] D. Maturana, P.-W. Chou, M. Uenoyama, and S. Scherer, "Real-time semantic mapping for autonomous off-road navigation," in *Field and Service Robotics: Results of the 11th International Conference*, pp. 335–350, Springer, 2018.
- [45] S. Huang, G. Xiong, B. Zhu, J. Gong, and H. Chen, "Lidar-camera fusion based high-resolution network for efficient road segmentation," in *2020 3rd International Conference on Unmanned Systems (ICUS)*, pp. 830–835, IEEE, 2020.
- [46] C. Li, S. Chen, Y. Zhao, and Y. Chen, "Road pavement identification based on acceleration signals of off-road vehicles using the batch normalized recurrent neural network," in *2019 IEEE International Conference on Artificial Intelligence and Computer Applications (ICAICA)*, pp. 172–177, IEEE, 2019.

- [47] T. Homberger, L. Wellhausen, P. Fankhauser, and M. Hutter, “Support surface estimation for legged robots,” in *2019 International Conference on Robotics and Automation (ICRA)*, pp. 8470–8476, IEEE, 2019.
- [48] B. Gao, A. Xu, Y. Pan, X. Zhao, W. Yao, and H. Zhao, “Off-road drivable area extraction using 3d lidar data,” in *2019 IEEE Intelligent Vehicles Symposium (IV)*, pp. 1505–1511, IEEE, 2019.
- [49] J. Mei, Y. Yu, H. Zhao, and H. Zha, “Scene-adaptive off-road detection using a monocular camera,” *IEEE Transactions on Intelligent Transportation Systems*, vol. 19, no. 1, pp. 242–253, 2017.
- [50] G. Reina, A. Milella, and R. Worst, “Lidar and stereo combination for traversability assessment of off-road robotic vehicles,” *Robotica*, vol. 34, no. 12, pp. 2823–2841, 2016.
- [51] C. H. ZHOU Mengru, G. H. XIONG Guangming, and L. Qingxiao, “Road traversability analysis of unmanned tracked platform in off-road environment,” *Acta Armamentarii*, vol. 43, no. 10, p. 2485, 2022.
- [52] C. Goodin, L. Dabbiru, C. Hudson, G. Mason, D. Carruth, and M. Doude, “Fast terrain traversability estimation with terrestrial lidar in off-road autonomous navigation,” in *Unmanned Systems Technology XXIII*, vol. 11758, pp. 189–199, SPIE, 2021.
- [53] T. Overbye and S. Saripalli, “G-vom: A gpu accelerated voxel off-road mapping system,” in *2022 IEEE Intelligent Vehicles Symposium (IV)*, pp. 1480–1486, IEEE, 2022.
- [54] Y. Zhao, P. Liu, W. Xue, R. Miao, Z. Gong, and R. Ying, “Semantic probabilistic traversable map generation for robot path planning,” in *2019 IEEE international conference on robotics and biomimetics (RO-BIO)*, pp. 2576–2582, IEEE, 2019.
- [55] T. H. Y. Leung, D. Ignatyev, and A. Zolotas, “Hybrid terrain traversability analysis in off-road environments,” in *2022 8th International Conference on Automation, Robotics and Applications (ICARA)*, pp. 50–56, IEEE, 2022.
- [56] Y. Li, Z. Yu, C. Choy, C. Xiao, J. M. Alvarez, S. Fidler, C. Feng, and A. Anandkumar, “Voxformer: Sparse voxel transformer for camera-based 3d semantic scene completion,” in *Proceedings of the IEEE/CVF conference on computer vision and pattern recognition*, pp. 9087–9098, 2023.
- [57] X. Zhu, W. Su, L. Lu, B. Li, X. Wang, and J. Dai, “Deformable detr: Deformable transformers for end-to-end object detection,” in *International Conference on Learning Representations*, 2021.
- [58] J. Y. Wong, *Theory of Ground Vehicles*. Wiley, 4th ed., 2008.
- [59] L. Gan, R. Zhang, J. W. Grizzle, R. M. Eustice, and M. Ghaffari, “Bayesian spatial kernel smoothing for scalable dense semantic mapping,” *IEEE Robotics and Automation Letters*, vol. 5, no. 2, pp. 790–797, 2020.
- [60] A. Kendall, V. Badrinarayanan, and R. Cipolla, “Bayesian segnet: Model uncertainty in deep convolutional encoder-decoder architectures for scene understanding,” *arXiv preprint arXiv:1511.02680*, 2015.
- [61] W. R. Vega-Brown, M. Doniec, and N. G. Roy, “Nonparametric bayesian inference on multivariate exponential families,” *Advances in Neural Information Processing Systems*, vol. 27, 2014.
- [62] A.-Q. Cao and R. De Charette, “Monoscene: Monocular 3d semantic scene completion,” in *Proceedings of the IEEE/CVF Conference on Computer Vision and Pattern Recognition*, pp. 3991–4001, 2022.
- [63] S. Song, F. Yu, A. Zeng, A. X. Chang, M. Savva, and T. Funkhouser, “Semantic scene completion from a single depth image,” in *Proceedings of the IEEE conference on computer vision and pattern recognition*, pp. 1746–1754, 2017.
- [64] L. Roldao, R. de Charette, and A. Verroust-Blondet, “Lmscnet: Lightweight multiscale 3d semantic completion,” in *2020 International Conference on 3D Vision (3DV)*, pp. 111–119, IEEE, 2020.



Zitong Chen received the B.S. degree in vehicle engineering from Chang'an University in 2022. He is currently pursuing the Master degree in mechanical engineering at the National Engineering Laboratory for Electric Vehicles, Beijing Institute of Technology. His research interests focus on developing embodied agents for unmanned ground vehicles operating in off-road conditions or unstructured environments.



Chao Sun received the B.S. and Ph.D. degree in Mechanical Engineering from Beihang University and Beijing Institute of Technology in 2010 and 2016, respectively. He was a postdoctoral researcher at the Energy, Controls, and Applications Lab in University of California, Berkeley, CA, USA. Currently, he is an Associate Professor at Beijing Institute of Technology, studying on automated and connected vehicles and hybrid electric vehicles.



Shida Nie received the Ph.D. degrees in vehicle engineering from the Jilin University, Changchun, China. He is currently an associate research fellow of vehicle engineering with the School of Mechanical Engineering, Beijing Institute of Technology. His research interests include autonomous driving, vehicle dynamics control, and vehicle simulation technology.



Chen Min received the Ph.D. degree in school of computer science from Peking University, Beijing, China, in 2024. He is currently an associate research fellow with the Research Center for Intelligent Computing Systems, Institute of Computing Technology, Chinese Academy of Sciences, Beijing, China. His research interest is in 3D computer vision, with a particular interest in 3D perception for autonomous driving and embodied intelligence.



Changjiu Ning received the B.S. degree in vehicle engineering from Beijing Institute of Technology, Beijing, China, in 2021. He is currently pursuing the Ph.D. degree in mechanical engineering at the National Engineering Laboratory for Electric Vehicles, Beijing Institute of Technology. His research interests include the planning and control of autonomous vehicles, the application of manifolds in unmanned vehicles, and deep learning.



Haoyu Li received the B.S. degree in vehicle engineering from Hefei University of Technology, China, in 2020. He is currently pursuing the Ph.D. degree at the National Engineering Research Center for Electric Vehicles, Beijing University of Technology, China. His research interests include computer vision, deep learning, vehicle-infrastructure cooperative systems and their application in autonomous and electric vehicles.



Bo Wang received the B.S. degree in vehicular technology from Tsinghua University, Beijing, China, in 2020. He is currently pursuing the Ph.D. degree in mechanical engineering at the National Engineering Laboratory for Electric Vehicles, Beijing Institute of Technology. His research interests include pedestrian trajectory prediction and motion planning for automated and connected vehicles.